The paper was published in the proceedings of the 11th International Conference on Physical Modelling in Geotechnics (ICPMG2026) and was edited by Ioannis Anastasopoulos. The conference was held from June 8th to June 12th 2026 in Zurich, Switzerland.

Experimental investigation of thermal performance of metakaolin concrete in heat-exchanging walls using 1g physical modelling

M. Hajialilue-Bonab
Professor, Department of Civil Engineering, University of Tabriz, Tabriz, Iran, hajialilue@tabrizu.ac.ir

A. Khosravi, E. Maleki Tabrizi
Graduate Student, Department of Civil Engineering, University of Tabriz, Tabriz, Iran, a.khosravi1401@ms.tabrizu.ac.ir, emad.malekitabrizi@gmail.com

S. Rahnema
Graduate Student, Department of Civil Engineering, Sharif University of Technology, Tehran, Iran, salar.rahnema@sharif.edu

ABSTRACT: The integration of Ground Source Heat Pump (GSHP) systems into retaining and foundation elements, known as Geothermal Energy Walls (GEWs), represents a sustainable approach to harnessing shallow geothermal energy for building heating and cooling. Despite the growing application of GEWs, the influence of thermally enhanced concrete materials on their heat exchange performance is not yet fully understood. This study experimentally investigates the thermal behavior of Retaining Geothermal Energy Walls (RGEWs) constructed with metakaolin-enhanced concrete using controlled 1g physical modeling. Two wall specimens, an Ordinary Concrete Wall (OCW) and a Metakaolin Concrete Wall (MCW), were tested under identical thermal loading conditions with a constant inlet temperature difference of 15°C. The results revealed that the incorporation of 10% metakaolin as a supplementary cementitious material improved both thermal conductivity and the system's overall heat transfer rate. The MCW exhibited approximately 8% higher soil temperature rise and a correspondingly greater heat penetration depth compared with the OCW, indicating enhanced effective thermal diffusivity and a greater capacity for near-field thermal diffusion. These findings highlight the dual benefits of metakaolin, which improves both mechanical strength and thermal performance, making it a promising additive for optimizing geotechnical structures integrated with GSHPs. The study provides benchmark data for validating future numerical simulations and supporting the development of design guidelines for next-generation thermo-active retaining systems.

1 INTRODUCTION

The escalating global demand for low-carbon Heating, Ventilation, and Air Conditioning (HVAC) systems has intensified the focus on utilizing the ground as a stable and sustainable heat source/sink (Unfccc, 2015). Shallow geothermal energy systems, often integrated with Ground Source Heat Pumps (GSHP), represent a key pathway for reducing reliance on fossil fuels and mitigating Greenhouse Gas (GHG) emissions from the building sector (Agreement, 2015). The integration of GSHP primary loops into a structure's geotechnical components, known as thermo-active geostructures, offers a novel and cost-effective approach to utilize elements required for structural support as efficient heat exchangers (Loveridge et al., 2015; Preene & Powrie, 2009). These primary loops consist of HDPE pipes embedded in elements like Geothermal Energy Piles (GEPs), base slabs, and diaphragm walls, circulating a heat-carrier fluid to exchange thermal energy with the ground mass (Akrouch et al., 2014; Park et al., 2013).

Among these geostructures, Geothermal Energy Walls (GEWs) are particularly relevant in large urban civil engineering projects, such as subway stations and multi-story underground parking, where they are used for excavation support (Barla et al., 2023; Dai et al., 2023). Notable real-world implementations include the U2 Metro Line Extension in Vienna, Austria (Brandl et al., 2006), and the Bvlgari Hotel in London, UK (Amis et al., 2010). A critical challenge in their design is the lack of standardized design codes; hence, current practices rely significantly on empirical data and scientific monitoring of executed projects (Adam & Markiewicz, 2009; Amis et al., 2010; Brandl et al., 2006; Katzenbach et al., 2016; Xia et al., 2012). Unlike GEPs, Retaining

Geothermal Energy Walls (RGEWs) are non-axisymmetric, with one side typically exposed to air (excavation) and the other in contact with soil, making their thermal behavior and analysis more complex.

The efficiency of the GSHP system is fundamentally dependent on the rate of heat exchange at the primary loop. Heat transfer between the circulating fluid and the surrounding soil involves a sequence of mechanisms: convection inside the pipe fluid, and primarily conduction through the pipe wall, the concrete infill, and the surrounding soil (Faizal et al., 2016). While soil properties, such as thermal conductivity, moisture content, and environmental factors including groundwater flow and initial ground temperature, significantly influence the overall heat flux, the thermal conductivity of the concrete mixture in the GEWs is a decisive parameter (Sani et al., 2019).

Efficient heat exchange in GEWs and other thermo-active structures is governed by the coupled effects of temperature gradients, flow dynamics, and material conductivity. Precise control of these factors is vital for enhancing system reliability and ensuring accurate evaluation through Thermal Response Tests (TRT). The maximum usable temperature and flow rate are crucial operational parameters; field analyses using TRT show that optimizing fluid flow rates (0.5 to 0.7 m/s) and maintaining specific temperature ranges (25°C to 30°C for heating) significantly enhances TRT accuracy and system efficiency (Hu et al., 2024; Zhong et al., 2020).

To overcome the inherent thermal resistance of concrete, prior researches have explored the use of various additives (Elkezza et al., 2024; Elkezza et al., 2022). Studies show that incorporating additive materials, such as graphite and Phase Change Materials (PCM), into the concrete matrix can significantly improve thermal performance. For instance, graphite-enhanced concrete has demonstrated up to 20% higher thermal efficiency in laboratory models (Elkezza et al., 2022). and PCMs can enhance thermal efficiency by up to 43% compared with standard concrete (Elkezza et al., 2024). However, there is a recognized gap in the empirical data regarding the application of novel, cost-effective Supplementary Cementitious Materials (SCMs), like metakaolin, for thermal enhancement in large-scale GEWs. Furthermore, achieving long-term thermal stability requires balancing heating and cooling cycles to prevent permanent thermal accumulation or depletion in the surrounding soil (Makasis & Narsilio, 2019).

This study aims to bridge the material knowledge gap by experimentally investigating the thermal behavior of RGEWs modified with Metakaolin. Metakaolin is a SCM widely used to enhance mechanical properties, but its direct impact on improving thermal performance in this context is novel. The primary objective is to evaluate the influence of replacing 10% of cement with metakaolin on the overall thermal response of the wall. To ensure reliable and realistic findings, a controlled laboratory-scale physical model was developed to simulate near-realistic boundary conditions, overcoming the limitations of oversimplified experimental setups and providing high-quality benchmark data for future numerical analyses.

The scope of this current physical modeling phase is strictly confined to evaluating transient thermal diffusion and localized temperature field distributions; assessments of complex hydro-thermal coupling and thermo-mechanical structural responses are not in the scope of this paper.

2 METHODOLOGY

The thermal performance analysis of RGEWs necessitates accurate and reliable data derived from controlled 1g physical modeling, offering a cost-effective alternative to full-scale field testing.

2.1 Material

Standard Firoozkooh sand (No. 161) was employed as the testing bed soil. Based on previous studies conducted on the physical and chemical characteristics of this sand (Irani et al., 2024; Jafarzadeh et al., 2023; Maleki Tabrizi et al., 2023; Rahnema & Jafarzadeh, 2024), it is composed of approximately 97% quartz, was selected due to the high thermal conductivity of quartz (7.7 to 8.4 W/m.K) (Fakharian et al., 2022), which enhances the thermal transfer capacity of the bed. The particle size distribution curve and the scanning electron microscope (SEM) image of grain morphology of the sand are illustrated in Figure 1. Key physical and mechanical parameters of the sand are presented in Table 1.

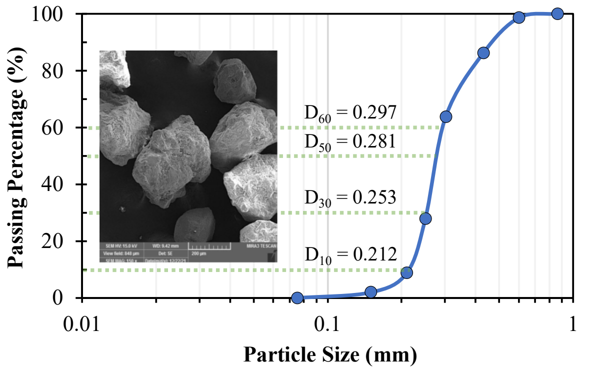

Figure 1. Particle size distribution curve and the SEM image of grain morphology of standard Firoozkooh sand (No. 161).

Table 1. Physical and mechanical properties of standard Firoozkooh sand (No. 161).

Parameters	G_s	e_{min}	e_{max}	ϕ	C_c	C_u
Value	2.65	0.54	0.94	33°	1.01	1.39

Due to laboratory-scale constraints (3 cm wall thickness), a fine aggregate-only mortar mix was utilized, while maintaining the structural design of a concrete wall. The mix design adhered to ACI 211.1 guidelines, with a Water-to-Cement (W/C) ratio of 0.5 and a maximum aggregate size limited to 4.75 mm. While the omission of coarse aggregates, which typically possess higher thermal conductivities than cement paste, may slightly reduce the absolute baseline thermal conductivity of the mix compared to a full-scale prototype, this geometric scaling constraint was applied equally to both the OCW and MCW specimens. Consequently, the systematic effect of this omission cancels out, ensuring that the relative thermal enhancement observed in the comparative analysis remains valid and unaffected.

A polycarboxylate-based superplasticizer (0.5% by cement weight) was used to ensure the mixture exhibited Self-Compacted Concrete (SCC) properties, achieving a flow spread of 16 to 18 cm (ASTM C1437) for proper mold filling. From a constructability perspective, the high specific surface area of metakaolin increases the cohesiveness and plastic viscosity of the fresh mix. While this enhanced cohesiveness is advantageous for preventing segregation and ensuring full encapsulation of pre-installed reinforcement cages, the increased viscosity could pose workability challenges in field applications where cages are pushed into pre-poured wet concrete. However, this rheological shift can be effectively managed on-site by optimizing the dosage of High-Range Water Reducers (HRWR) or superplasticizers, ensuring the material remains fully compatible with various field installation methods.

Two mixes were prepared using Type II Portland cement: Ordinary Concrete Wall (OCW), and Metakaolin Concrete Wall (MCW). The metakaolin concrete mix achieved a 28-day compressive strength of 33.5 MPa, a significant increase over the control mix (30.4 MPa), confirming the positive mechanical effect of metakaolin concrete. The specific mix proportions per cubic meter are summarized in Table 2.

To directly quantify the thermal enhancement of the mixtures and establish a material baseline, an in-house 1D transient heat conduction test was performed on radially insulated cylindrical specimens (20 cm height, 5 cm diameter). Heat was applied from a constant-temperature base, and temperatures were recorded along the central axis at depths of 5 cm, 10 cm, and 15 cm. The 1D transient Fourier equation was solved using the 5 cm and 15 cm measurements as time-dependent Dirichlet boundary conditions. A Particle Swarm Optimization (PSO) algorithm was employed to minimize the error between the measured and simulated midpoint (10 cm) temperatures, allowing for the precise extraction of the thermal diffusivity (α) for both mixes.

Table 2. Detailed mix proportions and material quantities for the ordinary and metakaolin concrete mixtures.

Component	Ordinary Concrete	Metakaolin Concrete
Water (kg/m³)	250.5	250.5
Cement (kg/m³)	501.0	451.0
Metakaolin (kg/m³)	0.0	50.0
Fine aggregate (kg/m³)	1406.0	1416.0
Coarse aggregate (kg/m³)	0.0	0.0
Superplasticizer (kg/m³)	2.5	2.5

2.2 Setup and Physical Model

The RGEW examined in this study consists of a reinforced concrete panel with a width of 28 cm, a thickness of 3 cm, a height of 70 cm, and an embedment depth of 20 cm in the laboratory model. Considering a geometric scaling factor of 1:20 and applying conventional similitude principles at 1g conditions. (Wood, 2004), the corresponding prototype dimensions in the field are equivalent to a wall 14 m in height.

To clearly establish the correspondence between the laboratory model and the full-scale prototype, the governing similitude relationships used in this study are summarized in Table 3. The scaling factors presented include geometric parameters of the wall (height, thickness), heating and recovery time and temperature. These parameters form the basis for interpreting the laboratory results in terms of field performance. Each scaling relation listed in the table will be further discussed in the following, where its role in model design, thermal loading, and heat-transfer behavior is elaborated in detail.

Table 3. Summary of relevant scaling factors (N = prototype/model)(Wood, 2004).

Quantity	Scale Factor	Model	Prototype
Wall Length	N = 20	70 (cm)	14 (m)
Wall Thickness		3 (cm)	0.6 (m)
Heating Time	N^2 = 400	12 (h)	200 (day)
Recovery Time		12 (h)	200 (day)
Temperature	1	15 (°C)	15 (°C)

As illustrated in Figure 2, the wall specimens were reinforced with a 3 mm diameter steel cage. The heat exchanger consisted of a W-shaped silicon tube (6 mm internal diameter, 1 mm wall thickness, 2.75 m total length), selected as the closest analog to real-scale HDPE pipes. The tube was centrally placed within the wall. Both wall specimens were cured for 28 days prior to testing.

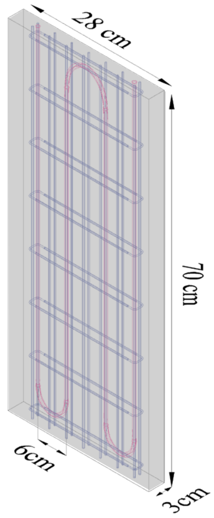

Figure 2. Cross-sectional details of the laboratory model of the RGEW and heat exchanger specifications.

The physical model was housed in a rigid steel box with a transparent Plexiglas front face for visual observation, as schematically illustrated in Figure 3. The container had internal dimensions of 140 cm in length, 30 cm in width, and 95 cm in height, providing sufficient space for controlled soil placement and thermal boundary development. Firoozkooh 161 sand was placed using the sand pluviation method in dry, successive layers to achieve a target relative density of 50%. While geothermal structures often interact with groundwater, this study specifically models a dry soil medium. This approach simulates the deep, dry vadose zones prevalent in arid and semi-arid urban environments where heat transfer is strictly conduction-dominated. Furthermore, utilizing standardized dry soil prevents complex, coupled thermo-hydraulic phenomena such as inhomogeneous moisture migration and latent heat transfer, allowing for the strict isolation, evaluation, and benchmarking of the concrete's independent thermal properties without advective interference.

The wall panel was installed after an initial 25 cm of sand placement and compaction to maintain an 8d clearance from the container bottom, minimizing boundary thermal effects. (Zhao et al., 2020).

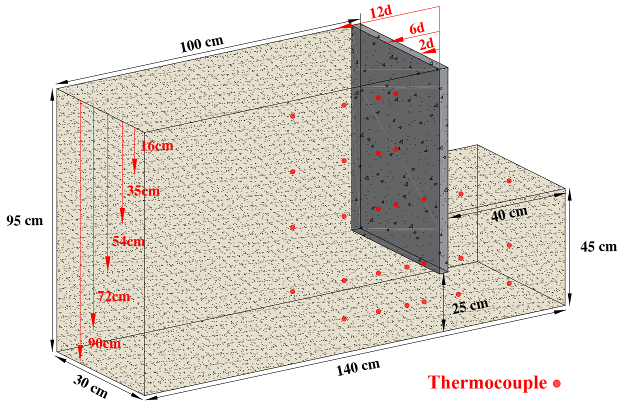

Figure 3. Schematic illustration of the physical model setup showing the container dimensions, wall panel position, and instrumentation layout.

As schematically presented in Figure 4, insulation boundary conditions were meticulously applied to the entire container to ensure controlled heat transfer pathways. All sides of the container were fully insulated using 6 cm of Styrofoam and fiberglass wool to minimize heat transfer to the laboratory environment. This configuration effectively imposed an adiabatic condition on the lateral boundaries, ensuring that heat flux was primarily unidirectional (in-plane) and that zero out-of-plane heat flux was maintained along the container's width, which is critical for accurate thermal analysis.

The exposed soil surface on the front (excavation side) was insulated with polyurethane foam and covered with fiberglass wool. This condition assumes that, after a brief initial heat exchange with the confined excavated space, the wall reaches thermal equilibrium with this space, resulting in negligible convective interaction and effectively establishing a zero heat flux boundary for the remainder of the experiment.

The surface boundary conditions for the back wall soil were configured to represent realistic field scenarios while ensuring isothermal behavior within the physical model. The back soil surface boundary was intentionally left uninsulated and exposed to ambient air, allowing natural and realistic simulation of ground–atmosphere heat exchange, where shallow soil layers remain in continuous thermal interaction with the surrounding climate. Because the ground surface temperature at this boundary rapidly equilibrates with ambient air and does not sustain a persistent temperature gradient, no dominant convective regime develops for which the Biot number would control heat transfer behavior.

Similarly, all insulated boundaries, including the wall surfaces not in direct contact with the soil, experience no external heat exchange, rendering the effective convection coefficient approximately zero. For these reasons, the Biot number is not considered a governing similitude parameter in this study, as it does not influence the thermal response of the modeled system.

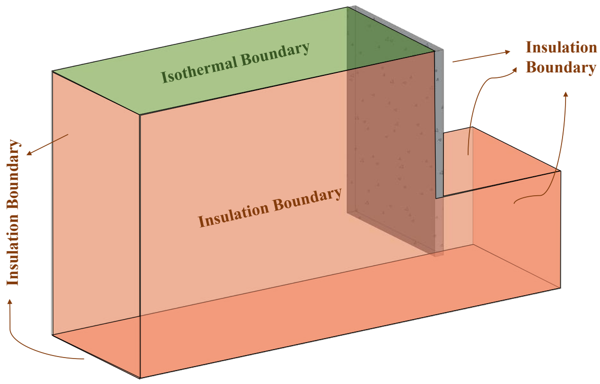

Figure 4. Schematic illustration of the thermal boundary conditions applied to the physical model.

A data-logging system equipped with 32 calibrated temperature sensors, each with an accuracy of 0.1°C, was utilized to continuously monitor the temperature at 10-second intervals. A thermally conductive silicone paste was applied to ensure proper sensor-concrete contact. The heating system operated under a constant fluid circulation rate of 0.7 L/min throughout the experiments. Before testing, the system was stabilized for 12 hours to establish the initial temperature ($T_{initial}$). Then a constant thermal load of $\Delta T = 15°C$ was applied for 12 hours by adjusting the inlet water temperature with continuous circulation, followed by 12 hours of recovery phase.

The duration of this thermal cycle was determined by maintaining the thermal similitude between the laboratory model and the field prototype, which is essential for accurately simulating transient heat flow. Since the primary heat transfer mechanism in the dry sand is conduction and the thermal properties of the model soil and the prototype soil are considered identical, the time scaling factor must satisfy the Fourier number (Fo) similitude ($Fo_{model} = Fo_{prototype}$) (Kramer et al., 2015). The Fourier number is defined by the ratio of conductive heat transfer rate to the rate of thermal energy storage as Equation (1).

$$Fo = \frac{\alpha t}{L^2} \quad (1)$$

where α (m^2/s) is the thermal diffusivity, t (s) is time and L (m) is characteristic length. The resulting relationship dictates that the time scale is proportional to the square of the geometric scale. Given the geometric scaling factor of 1:20, the time scaling factor is calculated as 1:400.

It is important to emphasize that heat transfer across the solid–solid interfaces of the system (i.e., between the pipe wall, concrete, and soil) is governed exclusively by conduction. Because the physical model utilizes the identical solid materials expected in the field prototype, the ratios of thermal conductivities (k_1/k_2) and diffusivities (α_1/α_2) across these interfaces are inherently 1:1. Therefore, the Fourier number remains the sole dimensionless parameter required for dynamic thermal similitude. Convective scaling via the Biot number (Bi) is not applicable to these internal solid boundaries, and the constant internal fluid circulation effectively imposes a steady Dirichlet boundary condition at the heat source.

Furthermore, because the experimental setup utilizes dry sand, the groundwater seepage velocity is zero ($v = 0$). Consequently, the advective Péclet number (Pe) evaluates to zero for both the physical model and the corresponding prototype, ensuring hydraulic-thermal similitude ($Pe_{model} = Pe_{prototype} = 0$) is perfectly satisfied without distortion.

Therefore, the 12-hour heating and 12-hour cooling periods conducted in the model are equivalent to 4800 hours (approximatly six months) of thermal loading and recovery, respectively, in the full-scale prototype. This ensures that the thermal diffusion and heat penetration depth achieved in the laboratory accurately reflect the operational behavior period in the field. Finally, two tests were conducted, one on the OCW and other one on the MCW, under identical thermal loading.

3 RESULTS AND DISCUSSION

The comparative analysis of the OCW and the MCW provides strong evidence of the effectiveness of metakaolin as a thermal enhancement additive for GEWs. The independent inverse thermal analysis yielded baseline thermal diffusivities of 1.13 mm^2/s and 1.24 mm^2/s for the OCW and MCW mixtures, respectively. Coupled with the measured dry densities (2045 kg/m^3 and 2041 kg/m^3) and specific heat capacities (927 J/kg·°C and 928 J/kg·°C), the thermal conductivity of the metakaolin concrete was determined to be 2.35 W/m·°C, representing a 9.8% increase over the ordinary concrete (2.14 W/m·°C). This fundamental material enhancement directly governed the system-level behavior observed in the physical model. The temperature variations measured within the soil at different horizontal distances from the wall are presented in Figure 5. The plotted temperature-distance profile clearly illustrates how thermal energy propagates from the heated concrete walls into the surrounding dry sand.

All reported results correspond to the sensors positioned along the mid-height of the soil layer. This elevation was deliberately selected to ensure that the sensors remained sufficiently distant from both the upper air-soil interface and the bottom boundary, thereby minimizing any boundary-induced thermal disturbances. By placing the sensors at this neutral depth, the measurements more accurately represent the true horizontal heat transfer from the wall without interference from vertical thermal gradients.

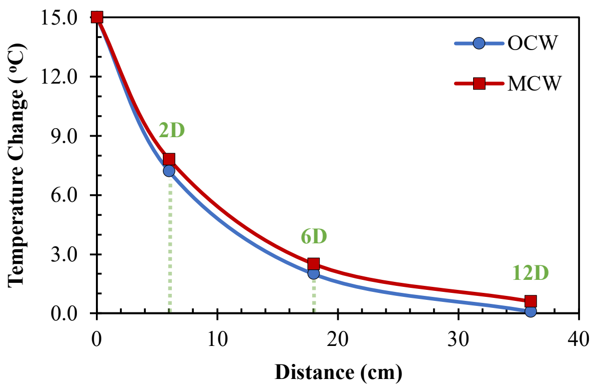

Figure 5. Temperature change in the surrounding soil at various horizontal distances from the OCW and MCW after 12 hours of heating.

The shape of the temperature attenuation curve further confirms that the system did not reach steady-state conditions during the 12-hour heating period. Instead, the non-linear decay of ΔT with increasing distance indicates a transient thermal regime, where the temperature field continues to evolve with time. In a true steady state, the temperature gradient would asymptote to a constant value at all distances (linear graph); however, the declining curve observed in both wall systems demonstrates that the transient front had not yet fully progressed through the soil domain.

The inclusion of metakaolin in the MCW had a notable influence on the soil's thermal response. As shown in Figure 5, the temperature change in the soil adjacent to the MCW is on average 0.5°C higher than that of the OCW at all measured distances. At the 6 cm (2d) location, the MCW produced a temperature rise of approximately 7.8°C, compared with 7.2°C for the OCW, showing an increase of about 8%.

Furthermore, the other measurements, 18 cm (6d), and even at the far boundary of 36 cm (12d), the MCW consistently exhibits higher ΔT values. Notably, at the 36 cm distance where the OCW's ΔT nearly approaches zero, the MCW still maintains a measurable temperature change. This observation confirms a deeper thermal penetration depth in the soil and implies a higher effective thermal conductivity for the MCW system. This difference reflects the enhanced thermal conductivity of the metakaolin concrete, leading to more efficient heat transfer through the soil.

It should be noted that in a series thermal resistance circuit, the high thermal resistance of the dry sand heavily dominates the system. In field conditions where soil might be saturated and its thermal conductivity increases, the relative thermal resistance of the concrete becomes a much larger proportional bottleneck. Consequently, minimizing the concrete's thermal resistance via metakaolin becomes even more critical in multiphase environments. Therefore, the 8% improvement in the thermal profile observed in this dry-soil model likely represents a conservative, lower-bound estimate of metakaolin's enhancement potential in saturated field conditions.

Moreover, the overall pattern of heat diffusion, higher soil temperatures near the back face and sustained higher temperatures at greater distances on the front insulated face, was consistent across both experiments. This confirms that while material properties (metakaolin) improve the magnitude of heat transfer, the boundary conditions imposed by the test setup remain the dominant factor controlling the distribution of heat in the far-field soil.

4 CONCLUSIONS

This experimental investigation successfully compared the thermal performance of OCW and MCW under simulated thermal loading. The findings provide quantitative validation for the use of metakaolin as a functional additive to enhance the efficiency of GSHP-integrated geotechnical structures. Metakaolin significantly enhances the heat transfer rate**,** leading to consistently higher soil temperature rises around the MCW compared with the OCW over the same time span and under identical heating conditions. While this study directly demonstrates an improvement in the near-field temperature distribution rather than whole-system COP, it proves that minimizing the concrete's thermal resistance is a viable material optimization strategy.

1) Greater thermal penetration depth was observed for the MCW, as measurable temperature changes persisted even at the 36 cm (12d) distance where the OCW's influence nearly vanished.
2) Enhanced effective thermal conductivity of the MCW allows greater utilization of the surrounding soil's thermal storage capacity.

The study supports the practical application of metakaolin in geothermal energy systems. Future work should focus on investigating the long-term thermo-mechanical stability of the MCW, performing life-cycle economic assessments, and validating these findings through full-scale field testing.

REFERENCES

Adam, D., & Markiewicz, R. (2009). Energy from earth-coupled structures, foundations, tunnels and sewers. *Géotechnique, 59*(3), 229-236. https://doi.org/10.1680/geot.2009.59.3.229

Agreement, P. (2015). UNFCCC, Adoption of the Paris agreement. COP. *25th session Paris, 30*, 1-25.

Akrouch, G. A., Sánchez, M., & Briaud, J.-L. (2014). Thermo-mechanical behavior of energy piles in high plasticity clays. *Acta Geotechnica, 9*(3), 399-412. https://doi.org/10.1007/s11440-014-0312-5

Amis, T., Robinson, C., & Wong, S. (2010). Integrating geothermal loops into the diaphragm walls of the Knightsbridge Palace Hotel project. *EMAP-Basements and Underground Structures*.

Barla, M., Insana, A., & di Caravacio, A. B. (2023). Lessons learnt from a full-scale installation of energy walls. Symposium on Energy Geotechnics 2023, https://doi.org/10.59490/seg.2023.517

Brandl, H., Adam, D., & Markiewicz, R. (2006). Ground-sourced energy wells for heating and cooling of buildings. *Acta Geotechnica Slovenica, 3*(1), 4-27.

Dai, Q., Zhang, D., & Li, Z. (2023). Mechanical assessment of energy wall in the long term. *Acta Geotechnica, 18*(1), 1-34. https://doi.org/10.1007/s11440-022-01579-5

Elkezza, O., Alhawat, M., Mohamed, M., & Khan, A. (2024). Experimental investigation on the use of PCM heat exchangers in Geo-energy piles and walls. *Geothermics, 119*, 102950. https://doi.org/10.1016/j.geothermics.2024.102950

Elkezza, O., Mohamed, M., & Khan, A. (2022). Performance of thermally enhanced geo-energy piles and walls. *Geothermics, 98*, 102274. https://doi.org/10.1016/j.geothermics.2021.102274

Faizal, M., Bouazza, A., & Singh, R. M. (2016). Heat transfer enhancement of geothermal energy piles. *Renewable and Sustainable Energy Reviews, 57*, 16-33. https://doi.org/10.1016/j.rser.2015.12.065

Fakharian, K., Kaviani-Hamedani, F., & Imam, S. R. (2022). Influences of initial anisotropy and principal stress rotation on the undrained monotonic behavior of a loose silica sand. *Canadian Geotechnical Journal, 59*(6), 847-862. https://doi.org/10.1139/cgj-2020-0791

Hu, S., Kong, G., Aboel-Naga, H., & Yang, Q. (2024). Thermomechanical response of field-scale energy wall under different heating operations. *Journal of Geotechnical and Geoenvironmental Engineering, 150*(3),06023011.https://doi.org/10.1061/JGGEFK.GTENG-12066

Irani, A. E., Hajialilue-Bonab, M., Assadi-Langroudi, A., & Tabrizi, E. M. (2024). Pore-pressure-dependent performance of rocking foundations. *Soil Dynamics and Earthquake Engineering, 183*, 108772. https://doi.org/10.1016/j.soildyn.2024.108772

Jafarzadeh, F., Afzal, S., & Rahnema, S. (2023). مدلسازی فیزیکی رفتار شمع حرارتی منفرد در خاک خشک , Physical modeling of the behavior of thermal pile in dry sand (in Persian). https://civilica.com/doc/2061406

Katzenbach, R., Leppla, S., & Choudhury, D. (2016). *Foundation systems for high-rise structures*. CRC press. https://doi.org/10.1201/9781315368870

Kramer, C. A., Ghasemi-Fare, O., & Basu, P. (2015). Laboratory thermal performance tests on a model heat exchanger pile in sand. *Geotechnical and Geological Engineering, 33*(2), 253-271. https://doi.org/10.1007/s10706-014-9786-z

Loveridge, F., Olgun, C. G., Brettmann, T., & Powrie, W. (2015). Group thermal response testing for energy piles. In.

Makasis, N., & Narsilio, G. A. (2019). Utilising Soldier Pile Retaining Walls as Energy Geo-Structures. In *Geotechnical Engineering in the XXI Century: Lessons learned and future challenges* (pp. 2898-2905). IOS Press. https://doi.org/10.3233/STAL190363

Maleki Tabrizi, E., Dibazar, A. A., Hajialilue-Bonab, M., Esmatkhah Irani, A., & Assadi-Langroudi, A. (2023). The Partially Drained Behaviour of Dense Fibre-Reinforced Sands. *Sustainability, 15*(23), 16286. https://doi.org/10.3390/su152316286

Park, H., Lee, S.-R., Yoon, S., & Choi, J.-C. (2013). Evaluation of thermal response and performance of PHC energy pile: Field experiments and numerical simulation. *Applied Energy, 103*, 12-24. https://doi.org/10.1016/j.apenergy.2012.10.012

Preene, M., & Powrie, W. (2009). Ground energy systems: from analysis to geotechnical design. *Géotechnique, 59*(3), 261-271.

Rahnema, S., & Jafarzadeh, F. (2024). بررسی تاثیر دمای شمع حرارتی بر روی ظرفیت باربری نهایی آن با استفاده از مدل فیزیکی 1g, Experimental evaluation of thermal pile temperature effects on its ultimate bearing capacity using a 1g physical model (in Persian). https://civilica.com/doc/2060479

Sani, A. K., Singh, R. M., Amis, T., & Cavarretta, I. (2019). A review on the performance of geothermal energy pile foundation, its design process and applications. *Renewable and Sustainable Energy Reviews, 106*, 54-78. https://doi.org/10.1016/j.rser.2019.02.008

Unfccc, V. (2015). Adoption of the Paris agreement. *Proposal by the President, 282*(2).

Wood, D. M. (2004). *Geotechnical modelling* (2.2 ed.). CRC press.

Xia, C., Sun, M., Zhang, G., Xiao, S., & Zou, Y. (2012). Experimental study on geothermal heat exchangers buried in diaphragm walls. *Energy and buildings, 52*, 50-55. https://doi.org/10.1016/j.enbuild.2012.03.054

Zhao, R., Leung, A. K., Vitali, D., Knappett, J. A., & Zhou, Z. (2020). Small-scale modeling of thermomechanical behavior of reinforced concrete energy piles in soil. *Journal of Geotechnical and Geoenvironmental Engineering, 146*(4), 04020011. https://doi.org/10.1061/(ASCE)GT.1943-5606.0002225

Zhong, Y., Narsilio, G., Makasis, N., Li, Z., & Aditya, G. (2020). Thermal response of energy soldier pile walls. *E3S Web of Conferences*